# Development of Computational Model for Multi-Point Environmental Release of Radionuclides

**Juryong Park[a], Siho Jang[a], Eung Soo Kim[a], Sung-yeop Kim[b*]**
[a]Seoul National University, Seoul, Republic of Korea
[b]Korea Atomic Energy Research Institute, Daejeon, Republic of Korea

**Abstract:** The importance of multi-unit accident of nuclear power plant (NPP) site has increased significantly since the Fukushima Dai-Ichi nuclear power plant accident. In this regard, research on multi-unit PSA is being actively conducted, and multi-unit Level 3 PSA is also being actively studied as the final stage of PSA. The existing Level 3 PSA codes can account for temporal differences in the release of radioactive materials, but not spatial differences. Although the effects of spatial differences in the release of radioactive material can diminish at large distances, radionuclide releases from different locations can affect the radiation exposure and health effects of the population in the vicinity of a nuclear power plant, for example inside the precautionary action zone (PAZ). Therefore, for a sophisticated multi-unit Level 3 PSA, it is very important to develop a multi-point release computational model and install it in the Level 3 PSA code. In this study, a multi-point release computational model was developed based on the Gaussian puff model. Since radioactive substances are considered, the developed model incorporates not only atmospheric dispersion and dry/wet deposition, but also radioactive decay. In addition, to overcome the speed disadvantages of the Gaussian puff model compared to the Gaussian plume model, a Compute Unified Device Architecture (CUDA) coding technique that can utilize graphics processing units (GPUs) was introduced.

**Keywords:** Level 3 PSA, Multi-unit PSA, Multi-point release, Offsite consequence analysis

## 1. INTRODUCTION

Recent advancements in nuclear safety highlight the need for advanced computational tools to model radionuclide dispersion accurately following nuclear accidents. Current Level 3 Probabilistic Safety Assessment (PSA) models, which account for temporal variations in radionuclide releases, still struggle with complexities from spatial offsets between nuclear power plant (NPP) units as noted by Bixler and Kim. [1]. These spatial differences complicate multi-source evaluations and affect release signatures from various accident scenarios.

This study utilizes an enhanced Gaussian puff model, leveraging Compute Unified Device Architecture (CUDA) and graphics processing Units (GPUs), better suited for managing multi-point sources typical in multi-unit nuclear accidents compared to traditional Gaussian plume models. Previous research by Santos et al. [2] demonstrated the feasibility and computational efficiency of GPU-based real-time Gaussian puff model. Developed method in this study, which conducts a single computation per thread and then applies parallel reduction techniques, significantly boosts computational speed and efficiency.

Moreover, by simulating detailed atmospheric interactions and multiple release points under varied meteorological conditions, this study aims to provide a comprehensive analysis of potential offsite radiological impacts. This study integrates high-resolution meteorological data (Local Data Assimilation and Prediction System: LDAPS) to address the spatial differences between multiple nuclear units, allowing for precise predictions of radionuclide dispersion patterns that consider both the spatial arrangement of sources and specific meteorological scenarios at each location.

This study not only addresses the complexities associated with modeling atmospheric dispersion across multi-unit nuclear sites but also highlights the critical role of advanced computational tools in enhancing the efficiency and accuracy of such analyses. By integrating high-resolution meteorological data and leveraging the power of parallel computing, it is able to manage the spatial variations effectively and simulate radionuclide dispersion more precisely. These capabilities are essential for assessing potential offsite radiological impacts accurately and rapidly, thus improving emergency preparedness and public safety strategies. The integration of GPU acceleration into our modeling approach marks a significant advancement in the capability to conduct detailed multi-unit analysis, underscoring the ongoing evolution in nuclear risk management.

## 2. METHODOLOGY

### 2.1. Fundamentals of Gaussian Puff Model

#### 2.1.1 Gaussian Puff Equation

Simulation of this study uses the Gaussian puff model to accurately describe the atmospheric dispersion of pollutants, with detailed tracking of each puff and radionuclide. The key equation in the model defines the concentration $C_{i,k}$ of radionuclide $k$ within puff $i$ at a point $(x, y, z)$ at time $t$ as follows [3]:

$$C_{i,k}(x,y,z,t) = \frac{Q_{i,k}(t)}{(2\pi^{3/2}\sigma_h^2\sigma_z)} exp\left[-\frac{1}{2}\left(\frac{x-x_i(t)}{\sigma_h}\right)^2\right] exp\left[-\frac{1}{2}\left(\frac{y-y_i(t)}{\sigma_h}\right)^2\right] exp\left[-\frac{1}{2}\left(\frac{z-z_i(t)}{\sigma_z}\right)^2\right] \quad (1)$$

Where:

- $Q_{i,k}(t)$ represents the mass of radionuclide $k$ in puff $i$ at time $t$,
- $\sigma_h$ represents the standard deviation of the dispersion of puff in the horizontal directions ($x$ and $y$),
- $\sigma_z$ is the standard deviation of the dispersion of puff in the vertical direction ($z$),
- $x_i(t)$, $y_i(t)$, and $z_i(t)$ are the coordinates of the center of puff $i$ at time $t$.

This formulation facilitates precise simulation of how individual puffs containing different radionuclides disperse in the atmosphere over time. The model dynamically updates the dispersion parameters $\sigma_h$ and $\sigma_z$ to accurately simulate the dispersal patterns and deposition processes under varying atmospheric conditions.

#### 2.1.2 Atmospheric Stability Category

In the atmospheric dispersion modeling, Gaussian puff model is employed in conjunction with the Pasquill-Gifford stability categories, which are instrumental for setting dispersion coefficients based on atmospheric conditions. These categories include A (very unstable), B (unstable), C (moderately unstable), D (neutral), E (stable), and F (very stable). For each of these categories, the coefficients $a_h$, $b_h$, $c_h$ for horizontal dispersion, and $a_z$, $b_z$, $c_z$ for vertical dispersion are summarized in Table 1 below [4]:

Table 1. Pasquill-Gifford Coefficients for Dispersion Calculation

| **Stability** | **Horizontal Direction $\sigma_h$** | | | **Vertical Direction $\sigma_z$** | | |
|---|---|---|---|---|---|---|
| | $a_h$ | $b_h$ | $c_h$ | $a_z$ | $b_z$ | $c_z$ |
| A | -1.104 | 0.9878 | -0.0076 | 4.679 | -1.172 | 0.2770 |
| B | -1.634 | 1.0350 | -0.0096 | -1.999 | 0.8752 | 0.0136 |
| C | -2.054 | 1.0231 | -0.0076 | -2.341 | 0.9477 | -0.0020 |
| D | -2.555 | 1.0423 | -0.0087 | -3.186 | 1.1737 | -0.0316 |
| E | -2.754 | 1.0106 | -0.0064 | -3.783 | 1.3010 | -0.0450 |
| F | -3.143 | 1.0148 | -0.0070 | -4.490 | 1.4024 | -0.0540 |

To determine the specific stability category, we utilize vertical temperature gradients as a key indicator, among other methods. The gradient method is outlined in Table 2, which specifies the ranges of vertical temperature gradients associated with each stability category [5]:

Table 2. Vertical Temperature Gradient Ranges for Stability Categories

| **Stability Category** | **Vertical Temperature Gradient (℃/100$m$)** |
|---|---|
| A | $\Delta T/\Delta z < -1.9$ |
| B | $-1.9 \leq \Delta T/\Delta z < -1.7$ |
| C | $-1.7 \leq \Delta T/\Delta z < -1.5$ |
| D | $-1.5 \leq \Delta T/\Delta z < -0.5$ |
| E | $-0.5 \leq \Delta T/\Delta z < 1.5$ |
| F | $1.5 \leq \Delta T/\Delta z$ |

These gradient ranges are critical for accurately determining the atmospheric stability and thereby refining the simulation of pollutant dispersion under various atmospheric conditions. Furthermore, the dispersion coefficients for horizontal and vertical dispersions are calculated using the following expressions:

- The horizontal dispersion coefficient, $\sigma_h$, is computed using the equation:

$$\sigma_h = exp(a_h + b_h \ln(x) + c_h(\ln(x))^2) \quad (2)$$

- Similarly, the vertical dispersion coefficient, $\sigma_z$, is calculated as:

$$\sigma_z = exp(a_z + b_z \ln(x) + c_z(\ln(x))^2) \quad (3)$$

### 2.1.3 Deposition and Decay Models

Deposition and decay mechanisms are significant for predicting pollutant interactions with the environment, key to understanding their effects on public health. Dry Deposition involves the removal of particles and gases from the air via gravitational settling or surface impaction, modeled by an exponential function that incorporates deposition velocity and the trajectory of puff, as shown in Equation (4) [6]:

$$Q_m(t + \Delta t) = Q_m(t)\, exp(-v_d dt/\Delta s) \int_s^{s+\Delta s} g(s')ds' \quad (4)$$

Here, $Q_m$ represents the mass of the pollutant in the puff, $v_d$ is the deposition velocity, and $s$ to $s$+$\Delta s$ denotes the path over which the deposition occurs.

Wet Deposition involves the scavenging of airborne pollutants by precipitation. This process is particularly dependent on the relative humidity and is modeled by adjusting the removal rate based on environmental conditions [7]:

$$\Lambda = 3.5 \times 10^{-5} \frac{RH - RH_t}{RH_s - RH_t} \quad (5)$$

where $RH$ is the relative humidity, $RH_t$ is the threshold humidity for precipitation to affect pollutant removal, and $RH_s$ is the saturation humidity. The rate at which pollutants are removed from the atmosphere through wet deposition is then calculated as:

$$Q(t) = Q_0\, exp(-\Lambda t) \quad (6)$$

Radioactive Decay addresses the natural decline in the quantity of radioactive pollutants through decay over time. The decay process is represented mathematically by:

$$N(t) = N_0\, exp(-\lambda t) \quad (7)$$

Here, $N_0$ is the initial quantity of the radionuclide, and $\lambda$ is the decay constant, which is specific to each radionuclide and indicative of its half-life.

## 2.2. Parallel Computing Techniques

### 2.2.1 Puff Advection

Puff advection, a key component in atmospheric dispersion modeling, involves updating trajectory and spread of each puff based on wind fields and atmospheric conditions, transforming an initial puff $p_{ij}$ (the $j$-th puff from the $i$-th unit) to its updated state $p'_{ij}$. Traditionally, advection calculations for each puff are processed sequentially in serial computing environments, which can be inefficient for the large number of puffs typically involved in atmospheric modeling.

By contrast, using parallel computing architectures allows advection calculation of each puff to be assigned to a separate thread, significantly enhancing computational efficiency. For instance, instead of processing 18 (3 units × 6 puffs) sequential operations for 18 puffs, parallel computing can handle these simultaneously in a single operation cycle, greatly reducing processing time and improving scalability. This method demonstrates substantial improvements in handling complex dispersion modeling tasks, optimizing both speed and accuracy.

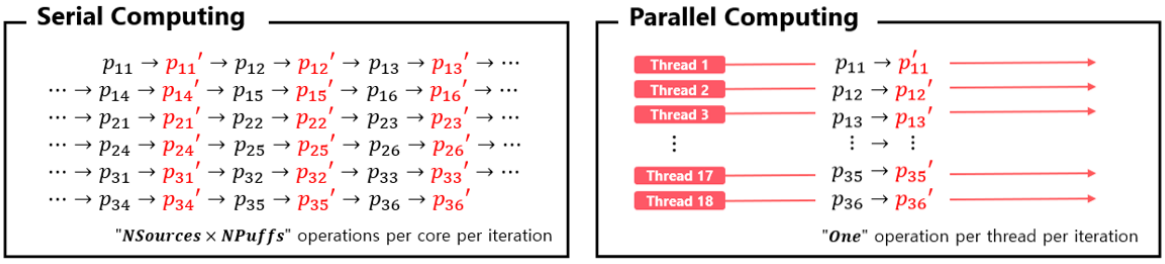


Figure 1. Serial vs. Parallel Computing for Puff Advection

The efficiency gains from parallel computing are particularly vital for handling large-scale simulations involving complex interactions over extensive geographic areas. Processing multiple puffs concurrently not only reduces the overall computational time but also allows for more dynamic and detailed atmospheric models to be run in shorter periods.

### 2.2.2 Concentration Summation

After calculating puff advection and diffusion, the next step is to sum the concentration impacts of all puffs on surrounding grid cells. For a scenario with 8,000 puffs affecting a 100×100 grid system of 10,000 cells, the computation demands are significant, traditionally requiring 80 million operations where the influence of each puff on each cell is calculated sequentially.

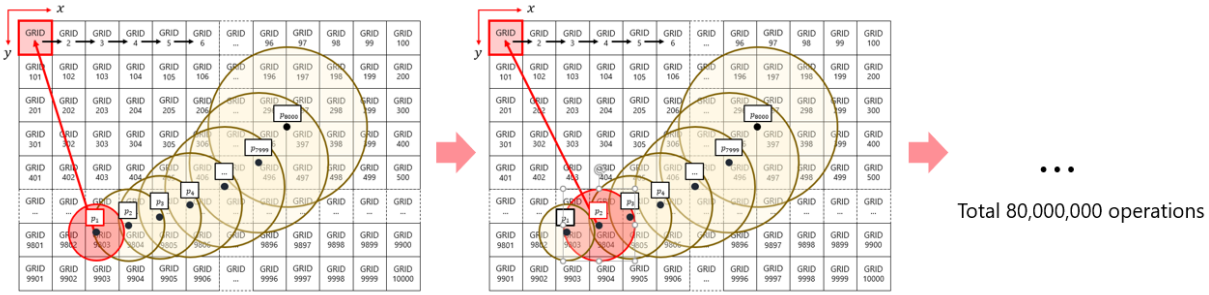


Figure 2. Overview of Sequential Operations in Concentration Summation

However, by employing parallel computing techniques, this massive computational challenge can be managed more efficiently. Each of the 80,000,000 concentration-grid interactions can be assigned to individual GPU threads, allowing for simultaneous processing where each thread handles a single operation. This approach is visually depicted in Figure 2, which illustrates the sequential operations, and Figure 3, which shows how these operations are managed in parallel.

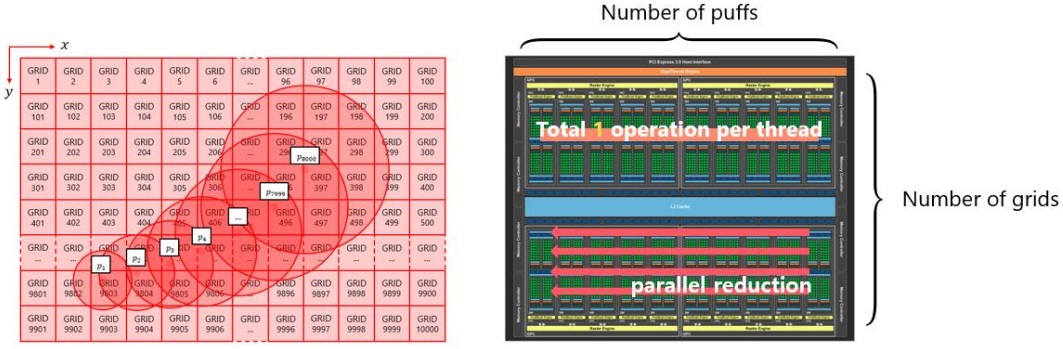


Figure 3. Overview of Parallel Operations in Concentration Summation

The computation of concentrations from thousands of puffs across grid cells is accelerated by parallel reduction techniques, which efficiently sum up values and reduce computational demand. This optimized computational method enables the handling of numerous scenarios simultaneously, making it highly suitable for application in Level 3 PSA, which requires managing extensive data sets.

## 3. RESULTS AND DISCUSSION

### 3.1. Model Validation

#### 3.1.1 Accuracy Verification Based on the Number of Puffs

In evaluating the accuracy of the GPU-accelerated Gaussian puff model, the primary goal was to determine the optimal resolution needed for accurate simulations by comparing its results with those of the Gaussian plume model. Under constant wind speed and direction, theoretical expectations hold that the results of puff model should approximate those of the Plume Model. To verify this, a series of tests varying the number of puffs from 6 to 6,000 was conducted under controlled conditions with specific parameters such as wind speed, emission rate, source height, and receptor plane detailed. This methodical approach ensured that each test provided reliable data for assessing the precision of puff model at different resolutions.

Table 3. Simulation Settings for Accuracy Verification Based on the Number of Puffs

| Parameter | Value |
|---|---|
| Wind speed ($u_x$, $u_y$, $u_z$) | (5 m/s, 0 m/s, 0 m/s) |
| Pasquill Category | C |
| Emission rate | 5.0e+6 μg/m$^3$ |
| Source height | 20 m |
| Receptor plane (x,z) | (300 m, 20 m) |

The outcomes of these simulations are illustrated in Figure 4, which plots the concentration distributions from the Gaussian puff model against the established curve of the Gaussian plume model. The initial simulations with only 6 puffs demonstrated noticeable deviations, with an $R^2$ value of 0.9845, indicating a lower correlation with the Gaussian plume model. However, increasing the number of puffs to 60 showed substantial improvement in model accuracy, and further increasing to 600 puffs achieved nearly perfect correlation, visually indistinguishable from the Gaussian plume and reflected by $R^2$ values approaching 1.0.

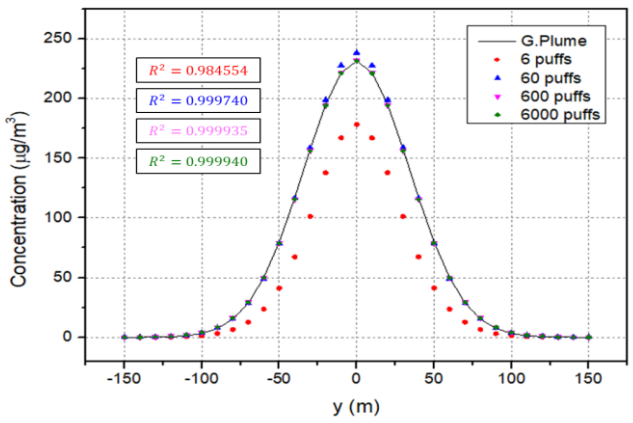


Figure 4. Dispersion Analysis of Gaussian Puff Models by Puff Quantity

Based on these results, it is recommended to use 600 or more puffs in simulations to ensure high fidelity in the Gaussian puff model outputs. This recommendation is supported by the marked increase in accuracy observed in the validation tests, particularly when the puff count reaches or exceeds 600. Such an approach not only ensures that the model predictions are reliable but also enhances the utility of model in conducting detailed atmospheric dispersion studies.

### 3.1.2 Validation Incorporating Dry/Wet Deposition and Radioactive Decay

After initial validation, the Gaussian puff model underwent further testing to assess its accuracy when incorporating environmental processes like dry deposition, wet deposition, and radioactive decay, which are important for realistic atmospheric dispersion modeling. The extended validation involved comparing the Gaussian puff model against the Gaussian plume model across various scenarios to ensure it could accurately predict dispersion with these additional environmental factors. Three specific cases were tested to measure the performance of model under different combinations of these processes.

- **Case 1** focuses on including dry deposition only.
- **Case 2** incorporates both dry and wet deposition.
- **Case 3** integrates dry deposition, wet deposition, and radioactive decay.

The results, depicted in Figure 5, show the concentration distributions for each case. The solid lines represent the outcomes of Gaussian plume model, while the dotted lines illustrate the results of Gaussian puff model. Remarkably, across all cases, the Gaussian puff model closely matched the Gaussian plume model, evidenced by high $R^2$ values approaching 1.0, indicating a strong correlation and accuracy of the puff model under enhanced environmental simulation conditions.

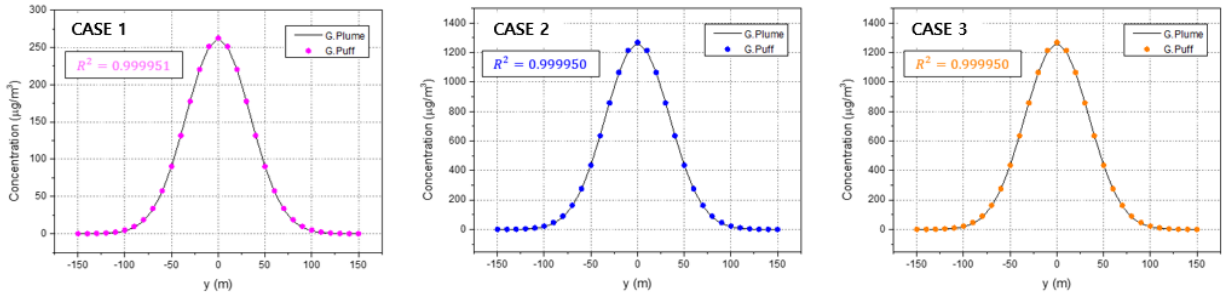


Figure 5. Accuracy of Gaussian Models with Dry/Wet Deposition and Radioactive Decay Cases

Additionally, the simulation settings used for these tests are detailed in the table below, which outlines parameters such as wind speed, Pasquill stability category, emission rate, source height, and the specific environmental processes included in each case.

Table 4. Simulation Settings for Dry/Wet Deposition and Radioactive Decay Cases

| Parameter | CASE 1 | CASE 2 | CASE 3 |
|---|---|---|---|
| Wind speed ($u_x$, $u_y$, $u_z$) | (5,0,0) m/s | (1,0,0) m/s | (1,0,0) m/s |
| Dry deposition velocity | 0.1 m/s | 0.1 m/s | 0.1 m/s |
| Relative humidity | - | 100% | 100% |
| Decay constant | - | - | 1.00e-6 /sec |
| Pasquill category | C | C | C |
| Emission rate | 5.0e+6 μg/s | 5.0e+6 μg/s | 5.0e+6 μg/s |
| Source height | 20 m | 20 m | 20 m |
| Receptor plane (x, z) | (300, 20) m | (300, 20) m | (300, 20) m |

### 3.1.3 Validation Across Different Atmospheric Stability Categories

After validating the Gaussian puff model for various environmental processes, its robustness was further tested against changes in atmospheric stability using parameters from Case 3. This validation phase assessed how well the model aligned with the Gaussian plume model across atmospheric stability categories B, C, D, and E. The results, depicted in the figure below, show that the puff model closely matches the predictions of plume model under all tested conditions, with concentration distributions for each category plotted as continuous lines for the plume and dotted lines for the puff.

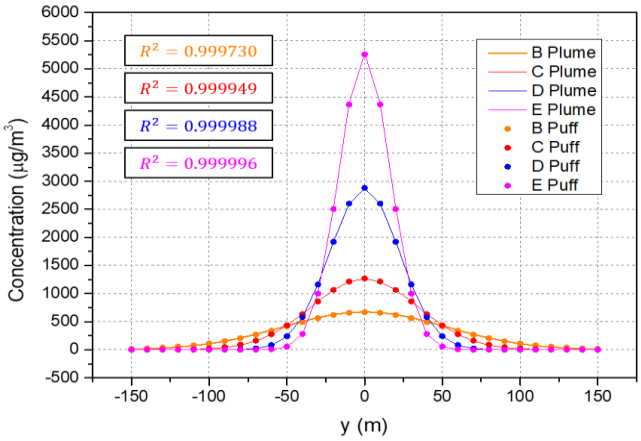


Figure 6. Comparison of Gaussian Plume and Puff Models Across Atmospheric Stability Categories

The $R^2$ values, indicating the correlation between the puff and plume models, were high in all cases, suggesting that the GPU-based Gaussian puff model can reliably replicate the expected dispersion patterns across a range of atmospheric stabilities.

### 3.2. Analysis of Multi-Unit Nuclear Accident Scenarios

#### 3.2.1 Simulation Setup

To evaluate the effectiveness of GPU-based Gaussian puff calculations in simulating a multi-unit nuclear accident, the following specific parameters and setup details were meticulously planned and executed. The simulations commenced on January 23, 2023, at midnight and continued for 1,200 seconds to model the initial dispersion phases post-accident. The setup involved Units 1 to 4 at the Wolseong NPP site, located at specific geographic coordinates, with emissions originating from an altitude of 20 meters. To capture the dynamic behavior of the plume, 8,000 puffs were simulated, providing a dense and detailed representation of the dispersion pattern. The atmospheric conditions were defined by the Pasquill-Gifford stability model, and a fine temporal resolution of 0.1 seconds was used to ensure high accuracy in tracking the evolution of plume.

The parameters were set as follows:

- **Time:** From January 23, 2023, at 00:00 for 1,200 seconds
- **Location:** Wolseong Nuclear Power Plant Units 1 to 4
- **Coordinates (longitude, latitude):**
  - Unit 1 (129.4761 *E*, 35.7131 *N*)
  - Unit 2 (129.4753 *E*, 35.7122 *N*)
  - Unit 3 (129.4739 *E*, 35.7106 *N*)
  - Unit 4 (129.4728 *E*, 35.7094 *N*)
- **Altitude of Sources:** 20 m
- **Number of Puffs:** 8,000

For a comprehensive analysis, various radioactive materials were considered, each characterized by specific decay constants, deposition velocities [8], and initial concentrations. This thorough setup allows for a detailed analysis of how different materials would behave and disperse in the event of an accident.

Table 5. Source Term Information for Multi-Unit Nuclear Accident Scenarios

| Source Term | Decay Constant | Deposition Velocity | Concentration [9] |
|---|---|---|---|
| Cesium - 137 | 7.28593e-10 /s | 1.0e-3 m/s | 2.74490741e+11 μg/m³ |
| Particulate Iodine | 1.00023e-6 /s | 1.0e-3 m/s | 2.97216435e+12 μg/m³ |
| Elemental Iodine | 1.00023e-6 /s | 1.0e-2 m/s | 2.97216435e+12 μg/m³ |
| Organic Iodine | 1.00023e-6 /s | 5.0e-4 m/s | 2.97216435e+12 μg/m³ |

### 3.2.2 Evaluating Dispersion Results from Multi-Unit Emissions

Exploring the impacts of various emission scenarios at a nuclear power plant provides critical insights into the potential risks and necessary mitigative strategies. The analysis began by simulating the dispersion of radioactive materials over time from different units within the Wolseong Nuclear Power Plant. Snapshots at specific times—300 seconds, 600 seconds, 900 seconds, and 1,200 seconds—illustrate the evolving dispersion pattern, clearly showing how the plume develops and spreads over the area.

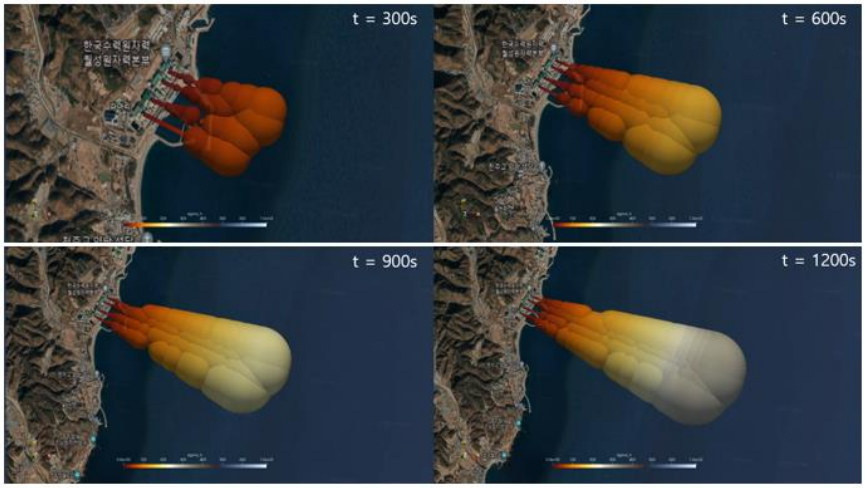


Figure 7. Time Evolution of Plume Dispersion

To further investigate multi-unit emissions, various scenarios were studied where different combinations of units were identified as the source of emissions. These scenarios were designed to simulate possible accident configurations and to determine how the distribution of radioactive material might differ based on the source units involved.

For instance, Case A analyzed emissions from Units 1, 2, and 3, while Case 5 considered emissions from Units 2 and 4. The graphical representations of these scenarios reveal significant variations in concentration distributions, highlighting the importance of considering the specific units involved in any potential incident.

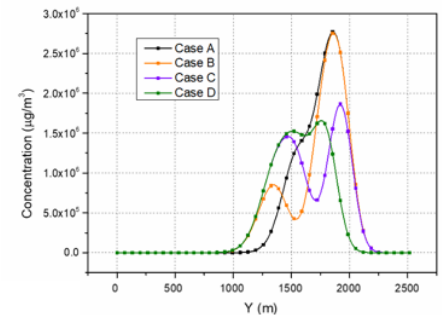


| Case | Emission Unit |
|---|---|
| **A** | 1, 2, 3 |
| **B** | 1, 2, 4 |
| **C** | 1, 3, 4 |
| **D** | 2, 3, 4 |

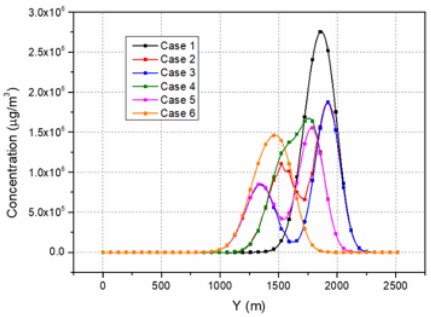


| Case | Emission Unit |
|---|---|
| **1** | 1, 2 |
| **2** | 1, 3 |
| **3** | 1, 4 |
| **4** | 2, 3 |
| **5** | 2, 4 |
| **6** | 3, 4 |

Figure 8. Concentration Distributions for Different Emission Scenarios

The comparison across different cases shows a clear dependency of dispersion patterns on the specific units emitting. For cases involving three units, the concentration peaks were higher and reached further distances, reflecting the increased volume of emissions. Conversely, scenarios with emissions from two units showed more localized dispersion patterns, emphasizing how the physical location of emissions critically influences the spread of contaminants.

This analysis underscores the importance of high-resolution atmospheric modeling in accurately predicting and managing the consequences of nuclear accidents involving multiple units, especially in the near-field. Such detailed studies are essential for emergency preparedness and response planning, especially in the closer emergency planning zone such as PAZ (precautionary action zone), ensuring that predictions are as accurate and useful as possible in real-world scenarios.

### 3.2.3 Evaluating Dispersion Results from Multi-Unit Emissions

Exploring the performance enhancements enabled by GPU acceleration in the Gaussian puff model, this section details the benchmarking process used to evaluate the execution times under various computational loads. The benchmarks were important in demonstrating how effectively the model scales with an increasing number of puffs and the substantial benefits of utilizing high-performance computing resources.

The benchmarks utilized a robust computational setup designed to handle intensive processing demands. This setup featured:

- **CPU:** Intel® Xeon® Silver 4210R CPU @ 2.40 GHz
- **RAM:** 250 GB
- **GPU:** NVIDIA GeForce RTX 3090, which plays a pivotal role in parallel processing tasks
- **Operating System:** Ubuntu 18.04.5 LTS
- **CUDA Toolkit:** Version 12.1, which supports advanced GPU functionalities

This high-level hardware configuration was instrumental in achieving the low execution times recorded during the simulations, even when handling large datasets such as the meteorological data from UM LDAPS with a resolution of 1.5km and a size of 2.0GB.

The execution time benchmarks were plotted to clearly show how the performance of model scales with increasing puff numbers, from 100 up to 12,800, focusing specifically on the calculations for puff advection and puff diffusion. These tests aimed to capture the minimal increase in execution time despite the substantial increase in computational load.

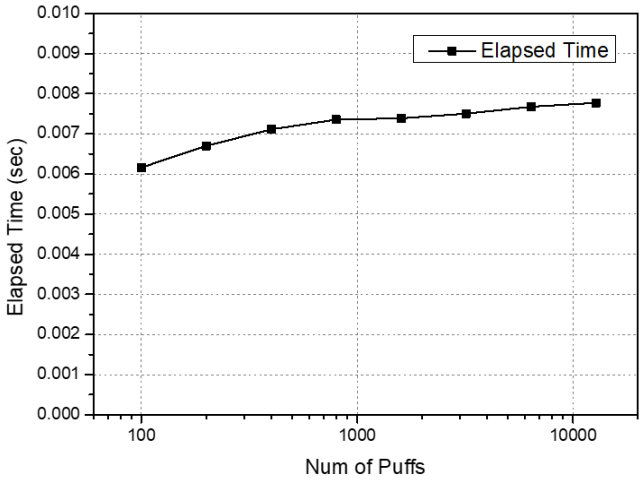


| Num of puffs | Elapsed Time (s) |
|---|---|
| 100 | 0.00616 |
| 200 | 0.0067 |
| 400 | 0.007113 |
| 800 | 0.007355 |
| 1600 | 0.007388 |
| 3200 | 0.007504 |
| 6400 | 0.007679 |
| 12800 | 0.007772 |

Figure 9. Execution Time Trends of the Parallelized Gaussian Puff Code

Further examination of the model's code highlighted the efficiency of GPU parallelization in managing computational loads. Even when the number of puffs was increased by a factor of 128, the execution time only increased by about 1.2 times. This minimal increase underscores the substantial benefits of utilizing GPU acceleration to handle large-scale simulations efficiently.

Additionally, the developed function significantly accelerated the iterative calculations for puff positions and physical properties, as well as the concentration computations at all grid points. Specifically, the function calculating concentrations demonstrated remarkable speed.

This rapid processing capability highlights how advanced hardware can drastically reduce computational times, thereby enhancing the feasibility of conducting detailed and high-resolution atmospheric dispersion simulations. Such capabilities are crucial for improving the accuracy and efficiency of environmental modeling, especially in scenarios that demand quick and accurate responses to potential atmospheric hazards.

## 4. CONCLUSION

This study aimed to enhance the modeling of atmospheric dispersion of radionuclides from multi-unit nuclear power plant accidents using a high-resolution Gaussian puff model. The research demonstrated significant advancements in atmospheric modeling by integrating the model with high-performance computing using CUDA and GPUs, allowing for more detailed and dynamic simulations of radiological releases.

Findings from this study confirm that the integration of the Gaussian puff model with advanced computational techniques and high-resolution meteorological data (LDAPS) enables precise simulations of atmospheric dispersion. The ability to model detailed dispersion scenarios with multiple emission sources significantly improves the accuracy of the impact assessments and enhances the speed of analysis. The computational model being developed can also account for release time differences between NPP units, and both spatial and temporal release differences will be considered in a practical analysis.

The model has been successfully validated across a variety of test cases and environmental conditions, including factors such as dry/wet deposition and radioactive decay. This validation confirms its robustness and reliability, demonstrating its ability to accurately predict dispersion patterns under different atmospheric conditions and emission scenarios.

The execution time benchmarks showcased the substantial computational advantages of GPU parallelization. Even with a significant increase in the number of puffs, scaling up by 128 times, the execution time increased only marginally, by 1.2 times. This underscores the efficiency of the parallel computing approach. The enhanced computational speed through parallelization is extremely useful and effective for processing a variety of scenarios in a Level 3 PSA context.

The enhancements introduced in this study significantly improve our capacity for conducting precise, efficient multi-unit analyses, essential for informed decision-making during potential nuclear incidents. The integration of high-resolution modeling techniques with advanced computational resources is advantageous for handling detailed multi-unit scenarios, where the scale and intricacy of potential accidents demand robust and reliable simulation tools. By refining and validating our model to adeptly manage the dynamics of these scenarios, it becomes a pivotal asset for strategic planning and advancing safety protocols within nuclear facilities.

**Acknowledgements**
This work was supported by a National Research Foundation of Korea (NRF) grant funded by the Korean government (MSIT: Ministry of Science, ICT) (No. RS-2022-00144405).

**References**

[1] Bixler, N. E., & Kim, S. Y. (2021). Performing a multi-unit level-3 PSA with MACCS. Nuclear Engineering and Technology, 53(2), 386-392.
[2] Santos, M. C., Pinheiro, A., Schirru, R., & Pereira, C. M. (2019). GPU-based implementation of a real-time model for atmospheric dispersion of radionuclides. Progress in Nuclear Energy, 110, 245-259.
[3] Ludwig, F. L., Gasiorek, L. S., & Ruff, R. E. (1977). Simplification of a Gaussian puff model for real-time minicomputer use. Atmospheric Environment (1967), 11(5), 431-436.
[4] Seinfeld, J. H., & Pandis, S. N. (2016). Atmospheric chemistry and physics: from air pollution to climate change. John Wiley & Sons.
[5] Mohan, M., & Siddiqui, T. A. (1998). Analysis of various schemes for the estimation of atmospheric stability classification. Atmospheric Environment, 32(21), 3775-3781.
[6] Hosker Jr, R. P. (1974). Estimates of dry deposition and plume depletion over forests and grassland. National Oceanographic and Atmospheric Administration, Oak Ridge, TN.
[7] Brandt, J., Christensen, J. H., & Frohn, L. M. (2002). Modelling transport and deposition of caesium and iodine from the Chernobyl accident using the DREAM model. Atmospheric Chemistry and Physics, 2(5), 397-417.
[8] Sportisse, B. (2007). A review of parameterizations for modelling dry deposition and scavenging of radionuclides. Atmospheric Environment, 41(13), 2683-2698.
[9] Jang, S., Park, J., Lee, H. H., Jin, C. S., & Kim, E. S. (2024). Comparative study on gradient-free optimization methods for inverse source-term estimation of radioactive dispersion from nuclear accidents. Journal of hazardous materials, 461, 132519.